Peer-reviewed version available at *Nanomaterials* **2018**, *8*, 881; doi:10.3390/nano8110881

Unravelling the thermal decomposition parameters for the synthesis of anisotropic iron oxide nanoparticles

Geoffrey Cotin[1,2], Céline Kiefer[1,2], Francis Perton[1,2], Dris Ihiawakrim[1,2], Cristina Blanco Andujar[1,2], Simona Moldovan[1,2], Christophe Lefevre[1,2], Ovidiu Ersen[1,2], Benoit Pichon[1,2], Damien Mertz[1,2] and Sylvie Begin-Colin [1,2,*]

[1] Université de Strasbourg, CNRS, Institut de Physique et Chimie des Matériaux de Strasbourg, UMR 7504, F-67034 Strasbourg, France

[2] Labex CSC, Fondation IcFRC/Université de Strasbourg, 8 allée Gaspard Monge BP 70028 F - 67083 Strasbourg Cedex.

Abstract. Iron oxide nanoparticles are widely used as contrast agent for MRI and may be used as therapeutic agent by magnetic hyperthermia if they display a high magnetic anisotropy. Considering the effect of the nanoparticles shape on anisotropy, the reproducible shape control of nanoparticles is currently a challenge of synthesis methods. By investigating reaction parameters which are the iron precursor structure, the water content and the amount of the surfactant, sodium oleate, reported to trigger the cubic shape, iron oxide nanoparticles with different shape and composition were observed to form. In particular, iron oxide nanoplates have been thus synthesized. The effect of the surfactant coming from precursor was taking into account by using in house iron stearates bearing either two or three stearate chains and the negative effect of water on shape was confirmed by considering these precursors after their dehydration. Nanocubes with straight faces and a $FeO@Fe_{3-x}O_4$ composition were obtained only with dehydrated precursors and 50% of sodium oleate in the oleic acid and sodium oleate surfactant mixtures. When iron stearates with three chains led mainly to nanocubes in presence of soduim oleate, Iron stearates with two chains led to the formation of nanoplates with 80% of sodium oleate. The original flat shape of the plates was confirmed with 3D TEM tomography. The investigation of the synthesis mechanisms confirmed the major role of deprotonated carboxylic acid and of the heating rate to drive the cubic shape of nanoparticles and showed that the nanoplate formation would depend mainly on the nucleation step and possibly on the presence of a given ratio of oleic acid and deprotonated carboxylic acid.

Introduction

The shape control of iron oxide nanoparticles (IONPs) is currently considered as promising to enhance the effective anisotropy and/or surface energy of IONPs which are required for given applications. Indeed, modifying the shape of the NPs will have different impacts. Specific shapes will be enclosed by different crystallographic planes that present different surface energies. The NPs with specific surface energy is rather important as catalytic applications will look for high energy surfaces[1,2]. They find applications also as biosensors[3]. Anisotropic shapes interest didn't rely only on the surface energy. Modifying the morphology will also have an impact on the magnetic properties by adding shape anisotropy to the NPs effective anisotropy. Bergstrom *et* al have demonstrated that even nanocubes displayed a shape anisotropy[4]. Therefore, IONPs with anisotropic shape have been investigated for biomedical applications and especially for magnetic hyperthermia and MRI applications[5–7]. Among the most interesting shaped IONPs are nanocubes and octopod shaped NPs. Nanocubes of 19 nm have been shown to be very good heating agents for therapy by magnetic hyperthermia[8]. It has been shown that the cubic morphology boosted the magnetic properties of IONP[4,8–10]. Furthermore, NPs with faceted shapes exhibited very high contrast enhancement properties promising for imaging by MRI[11–13]. Octopod IONPs were demonstrated to be high-performant T_2 contrast agents for magnetic resonance imaging[13].

However, the reproductible control of the NPs shape is not an easy task and remains a challenge. Among current synthesis methods, the thermal decomposition (TD) one is the most developed to tune the size and shape of IONPs. It involves the thermal decomposition of an iron precursor in presence of ligands in an organic solvent[14,15]. Commonly, iron precursors such as acetylacetonates[4,16,17], acetates[4] or oleates[14–16,18] have been decomposed in organic solvents containing surfactants. The strength of this method comes from the possibility to easily separate the NPs nucleation and growth steps following the theory of nucleation-growth proposed by Lamer[19]. The ligands used, which are mainly carboxylic acid or amine-based ligands, *in situ* coat the NPs during the synthesis process and allow controlling the growth step and prevent NPs from aggregation. They have also been shown to contribute to the stabilisation or destabilisation of the iron precursor[20,21]. The separation of nucleation and growth steps provided by the thermal decomposition method is the key parameter as it allows by playing on synthesis parameters to tune the size and shape of NPs.

The first admitted parameter to tune the shape was the nature of ligands. The role of the ligands, which was at first to stabilize colloidally the NPs in solution, was then to direct the growth of the nuclei towards anisotropic shapes[4,17,22,23,24,25]. A lot of studies have been then published on the effect of surfactants on the shape[6,7,12,13,26,27]. Kovalenko et al[17] reported at first the synthesis of nanocubes by decomposing an iron oleate precursor using an oleate salt as ligand. More recently, nanocubes have been synthesized by thermal decomposition in

Preprints (www.preprints.org) | NOT PEER-REVIEWED | Posted: 1 October 2018 doi:10.20944/preprints201810.0006.v1

Peer-reviewed version available at *Nanomaterials* **2018**, *8*, 881; doi:10.3390/nano8110881

dibenzylether (DBE) as solvent in presence of non-chelating ligands such as oleic acid.[28,29] Guardia et al[29] demonstrated that the shape control was induced by the product of decomposition of DBE at high temperature. While most of the reports emphasize the role of the ligands, Kim[28] underlined also the role of a kinetically controlled growth under high monomer concentration. Currently, most published results on the synthesis of nanocubes are based on the Kovalenko's method using different combination of ligands (NaOl/OA[10,27,30–32] – OA/OAm[33] – OA/ 4-Bisphenyl carboxilic acid[28,34]) and iron precursors mainly iron oleate or iron acetylacetonate. Few papers reported the synthesis of iron oxide nanoplatesby the thermal decomposition methods. Zhou et al[12] succeeded in the synthesis of cubes and plates among other shapes of IONPs by varying the ratio FeOl/NaOl and the reaction temperature. We recently demonstrated that the water content was an important parameter to control the cubic shape as it involved NaOl in micelles affecting their available amount to drive a specific growth[35]. There are many protocols for the synthesis of anisotropic shapes and every protocol differed from the other involving different heating rates, different ligands, and different concentration as illustrated in Table 1.

Unfortunately, no defined trend came out from the literature. There are as many protocols of nanocubes synthesis as there are publications. As various precursors, ligand combinations and solvents are used, no general rule came out. Yet what is often commented in the published works is that the ligands used in the synthesis and the heating rates appeared to be the main parameters for the shape control. However, the synthesis mechanism of anisotropic shape is not yet clearly understood.

In our group core@shell FeO@$Fe_{3-x}O_4$ nanocubes[36,37] were previously synthesized by adapting the Kovalenko's method[17] (sodium oleate and oleic acid ratio 3.6:1) using an *in house* iron oleate precursor. Nevertheless, the shape quality of nanocubes was highly dependent on the iron oleate batch and several iron oleate batches were often synthesized without succeeding in obtaining homogeneous nanocubes[35]. Replacing iron oleate by a commercial iron stearate led to shape heterogeneity. By synthesizing *in house* iron stearates bearing either two ($FeSt_2$) or three ($FeSt_3$) stearate chains and either hydrated or dehydrated, we showed that the hydration rate of iron stearates was crucial. Nanocubes with straight faces were obtained only with dehydrated iron stearates. That was explained by different thermal stability of stearates and kinetic considerations of the monomer generation. The so obtained structure of stearates was shown to have a great effect on the stability of the precursor against temperature and thus on the germination and growth steps. Nevertheless, the composition of these nanocubes as with iron oleate was core-shell FeO@$Fe_{3-x}O_4$. One may notice that very few papers dealt with the influence of the iron precursor structure on the formation of anisotropic shape by the thermal decomposition method. The pioneer work of Bronstein *et al*.[18,38] pointed at the role of the precursor structure which would be affected by washing solvents supported by Buck *et al.* that reported on the role of the precursor with the study of cobalt oleate ($CoOl_2$)[39].

Considering that the synthesis of anisotropic shaped NPs is very important due to their enhanced properties, the understanding of their synthesis mechanisms is still challenging. In that context and based on our previous investigations[35,45], we propose to investigate the effect of the structure of the precursor which has been poorly studied up to now and of the amount of soduim oleate on the nanoparticle shape. That's why in this work, four precursors, hydrated and dehydrated $FeSt_2$ and $FeSt_3$, have been decomposed in anisotropic conditions from an adapted Kovalenko's method[36]. Some important reported parameters have been thus investigated to better understand the mechanism addressing the shape of NPs: the influence of the structure (and hydration degree) of iron stearate, the ratio sodium oleate/oleic acid (NaOl/OA) and the heating rate. Then the nanoparticles with cubic, octopod and nanoplate shapes have been structurally characterized.

Table 1. Some reported nanocubes syntheses from litterature

Ref.	Precursor	Solvent	Ligand	Reflux T and duration	Heating rate	Observations
24	$Fe(acac)_3$	DBE	OA	290 °C / 30'	20 °C/min	Size and shape control with time and quantity of DBE
	$Fe(acac)_3$	DBE	OA / 4-Bisphenyl carboxilic acid	290 °C / 30'	20 °C/min	Smaller cubes
9	$Fe(Ol)_3$	OD or TOA	OA	340°C / 4h	10-15 °C/min	Size controled with T
30	$Fe(acac)_3$	DBE	OA / 4-Bisphenyl carboxilic acid	290 °C / 30'	ND	
25,26	$Fe(Ol)_3$	Squalane	NaOl / OA	315 °C / 2h	20 °C/min	Core-shell
29	$Fe(acac)_3$	DBE	OA / HDD /OAm	290 °C / 1h	15 °C/min	If heating rate increases along shorter reflux bigger NPs; on the opposite smaller NPs
7	$Fe(Ol)_3$	eicosane	NaOl / OA	350 °C / 30'	3,3 °C/min	Core-shell
35	$Fe(Ol)_3$ in situ	OD	NaOl	315 °C/ 2h	ND	Shape control through amount of NaOl
36	$Fe(Ol)_?$	OD	OA	320 °C / 30 '	5,5 °C/min	

[12]	$Fe(Ol)_3$	OD	NaOl / OA or DBAOL	315 °C / 30'	3,3 °/min	
[27]	$Fe(Ol)_3$	OD	NaOl /OA	315 °C / 30 '	4 °C/min	Ratio Fe(Ol)/NaOl control the size
[28]	$Fe(St)_2$	OA	NaOl /OA	380 °C / 2h	5 °C/min	
[23]	$Fe(acac)_3$	Squalane	Decanoic acid / DBE	310 °C / 1h	7 °C /min	Size controled with ratio squalane/DBE

Experimental Details

Synthesis Methods

Synthesis of iron stearate precursors Iron stearate (II) and (III) were prepared by precipitation of sodium stearate and ferrous chloride or ferric chloride salts in an aqueous solution. Briefly, sodium stearate (9.8 g, 32 mmol) was transferred into a 2 necked to a round bottomed flask (RBF) and solubilized in distilled H_2O (dH_2O, 80 ml). The solution is heated to reflux and stirred for 30 min until complete dissolution of the stearate. Separately, $FeCl_2.4H_2O$ (3.16 g, 16 mmol) or $FeCl_3.6H_2O$ (2,88 g, 16 mmol) was dissolved in dH_2O (40 ml) and added onto the sodium stearate solution under vigorous stirring. A light orange precipitate is formed immediately. The solution is kept under stirring at this temperature 15 min. Thereafter the solution is allowed to cool down to room temperature (RT). The obtained precipitate is washed once by centrifugation (hot dH_2O, 14000 rpm, 10 min). The product is then filtrated with a büchner funnel and oven dried at 65 °C for 24 h.

NPs Synthesis 2,32 mmol of iron stearate is mixed with 3 mmol of ligands (OA and NaOl at different ratios) in 15 mL OD. The mixture is stirred and heated at 120 °C for 60 min without reflux condenser in order to dissolve the reactants and remove the water residues. The cooler is then connected to the flask and the solution is heated up to 200 °C for 10 min with a heating rate of 5 °C/min. The solution is then heated up to 315 °C with a heating rate of 1 °C/min and refluxed for 60 min under air. After cooling to RT, a black and viscous suspension is obtained which is solubilized in 10 ml of chloroform. The NPs are then precipitated by the addition of an excess of acetone the first time and washed three times with chloroform and acetone at a ratio of 1:4 at 14000 rpm for 5 min by centrifugation. The NPs can finally be suspended in 50 ml of THF.

Synthesis of optimized cubes Iron oxide nanocubes (NC) were synthesised from iron stearate (III). Iron (III) stearate (2.72 g, 3 mmol) was mixed with OA (0.45 g, 1.5 mmol) and NaOl (0.45 g, 1.6 mmol) in eicosene (15 ml) in a two neck- RBF. The mixture was heated to 120 °C under stirring and kept at this temperature for 30 min without reflux condenser in order to dissolve the reactants and remove the water residues. The condenser was then connected to the flask and the solution heated to boiling temperature (≈343 °C, 15 °C/min). The solution was kept at reflux for 90 min under air. After cooling to RT, a black gel was obtained. The NPs were washed as previously described.

Synthesis of octopods Iron oxide Nano-octopods (NO) were synthesized from commercial iron stearate (III). Iron (III) stearate (0.735 g, 0.9 mmol) was mixed with OA (1.02 g, 3.6 mmol) in DBE (20 mL) in a two neck-RBF. The mixture heated at 120 °C under stirring and kept at this temperature for 60 min without reflux condenser in order to dissolve the reactants and remove the water residues. The condenser was then connected to the flask and the solution heated to 250 °C (5 °C/min) and kept at this temperature for 60 min. The solution was then brought to 320 °C (10 °C/min) and kept at reflux temperature for 60 min under air. After cooling to RT, a black solution was obtained. The NPs were washed as previously described.

Characterization methods

NPs were characterized by transmission electron microscopy (TEM) with a JEOL 2100 microscope operating at 200 kV (point resolution 0.18 nm). The size distribution of NPs was calculated from the size measurements of more than 300 nanoparticles using ImageJ software.

The X-ray diffraction (XRD) pattern was recorded at room temperature with a Bruker D8 Advance diffractometer equipped with a monochromatic copper radiation source (Kα = 0.154056 nm) and a Lynx-Eye detector in the 27-65°(2θ) range with a scan step of 0.03°. High purity silicon powder (a = 0.543082 nm) was systematically used as an internal standard. Profile matching refinements were performed through the Fullprof program[42] using Le Bail's method[43] with the modified Thompson-Cox-Hasting (TCH) pseudo-Voigt profile function.

Standard Infrared spectra were recorded between 4000 and 400 cm^{-1} with a Fourier transform infrared (FTIR) spectrometer, Spectrum 100 from Perkin Elmer. Samples were gently ground and diluted in non-absorbent KBr matrixes.

Results

Influence of the structure of precursors and sodium oleate ligand

$FeSt_2$ and $FeSt_3$ have been synthesized by a coprecipitation method using $FeCl_2.4H_2O$ and $FeCl_3.6H_2O$ respectively and these stearates have been heat-treated at 140°C for 48h to remove main crystallized water molecules leading to partially dehydrated stearates ($FeSt_{3,d}$ and $FeSt_{2,d}$)[35]. All stearates are mainly composed of Fe^{3+} but their structure differed due to the different amount of stearate ligand and different Fe III-carboxylate coordinations (a mixture of bridging and chelating coordinations). It was shown that the thermal stability of the different iron stearates is highly dependent on their structure as well as on their hydration degree[35].

Spherical and cubic iron oxide NPs have been then synthesized by thermal decomposition of these precursors in presence of surfactants in a high boiling solvent. These precursors have been decomposed using two standard protocols: one for the synthesis of 10 nm sized spherical nanoparticles (with oleic acid as surfactant and in dioctyl ether (B_p =290°C)) and the other one for the synthesis of nanocubes (with a mixture of oleic acid and sodium oleate as surfactant and in octadecene (B_p =315°C))[35]. The size of nanosphere was found to depend on the water content as well as the cubic morphology and the nanocube size[35]. The nanocube morphology was only obtained with dehydrated iron stearates and the nanocube size was larger with $FeSt_{3,d}$ (16 nm) than with $FeSt_{2,d}$ (10 nm). We suggested that the presence of water makes that oleates, used to drive the cubic shape, form micelles instead of stabilizing specific faces of nuclei. That would explain that the cubic morphology is observed when the water content is low. The nanosphere and nanocube sizes were related to the iron stearate decomposition kinetics: $FeSt_2$ and $FeSt_{2,d}$ decomposed in larger amount at lower temperature than $FeSt_3$ and thus favor the nucleation instead of the growth step[35]. In addition, if the composition of nanospheres was homogeneous, that of nanocubes is heterogeneous with a core-shell composition wüstite@magnetite: $Fe_{1-x}O@Fe_{3-x}O_4$. A further investigation of the decomposition mechanism of iron stearates demonstrated that the nucleis were composed of wüstite $Fe_{1-x}O$ and the final formation of the spinel phase was related to the oxygen diffusion up to the core which was found to depend on ligand-ligand interaction at the surface of NPs. Indeed the ligands monolayer at the surface of NPs may hinder the oxygen diffusion as it was observed with cobalt NPs coated with dodecanoic acid[44]. Depending on the nature of solvent or the reacting temperature, these interactions may be perturbated permitting the oxygen diffusion[45] (to be published results).

Considering the important role of the water content which would affect the amount of sodium oleate available to drive a cubic growth and a possible effect of the structure of iron stearate, the hydrated and dehydrated stearates have been here decomposed according to a previously published nanocube synthesis protocol[36] adapted from the Kovanlenko method[17] and different ratios of NaOl and OA (keeping the same total molar amount of ligands, only the ratio is varied) were tested. The synthesis involved a quick heating (5 °C/min) to a step at 200 °C for 10 min which is applied to favor the nucleation of NPs (improving the homogeneity of the mean size[20]) and then the reactant mixture is heated up to 315 °C with a heating rate of 1 °C/min and refluxed for 60 min under air. The same batch of iron precursors was used for the five tested ratios. Figure 1 showed TEM images of NPs obtained by tuning the type of iron stearates and the amount of NaOl. The main results are summarized in Table 2.

Table 2. Size and shape of nanoparticles as a function of the nature and amount of reactants (M Majority, m minatory, r rare)

Precursor		**0/100**	**20/80**	**50/50**	**80/20**	**100/0**
$FeSt_2$	Size (nm)	9.4 ± 1.9	11.7 ± 2.5	13.5 ± 2.5	17.5 ± 4.4 (L) 6.3 ± 1.3 (t)	7.2 ± 2.4
	Shape	*Spheres*	*Quasi octahedron*	*Deformed Cubes*	*Plates*	*Faceted*
$FeSt_{2,d}$	Size (nm)	10.0 ± 1.5	10.9 ± 1.4	10 ± 0.6	13.5 ± 5.2 (L) 6.5 ± 1.7 (t)	9 ± 2.7
	Shape	*Spheres*	*Quasi spherical*	*Cubes*	*Plates*	*Various faceted plates*
$FeSt_3$	Size (nm)	10.8 ± 1.7	12.4 ± 1.7	8.3 ± 2.2	11.3 ± 4.3	11.7 ± 1.5
	Shape	*Spheres*	*Quasi spherical*	*Faceted*	*Faceted*	*Cubes*
$FeSt_{3,d}$	Size (nm)	9.2 ± 1.5	9.8 ± 1.4	15.3 ± 1.8	20 ± 1.9/14 ± 1.4	13.9 ± 2.2
	Shape	*Spheres*	*Quasi spherical (M) / Octahedrons (r)*	*Cubes*	*Cubes (M)/Plates (m)*	*Elongated cubes*

*For plates : L for length and t for thickness.

Preprints (www.preprints.org) | NOT PEER-REVIEWED | Posted: 1 October 2018 doi:10.20944/preprints201810.0006.v1

Peer-reviewed version available at *Nanomaterials* **2018**, *8*, 881; doi:10.3390/nano8110881

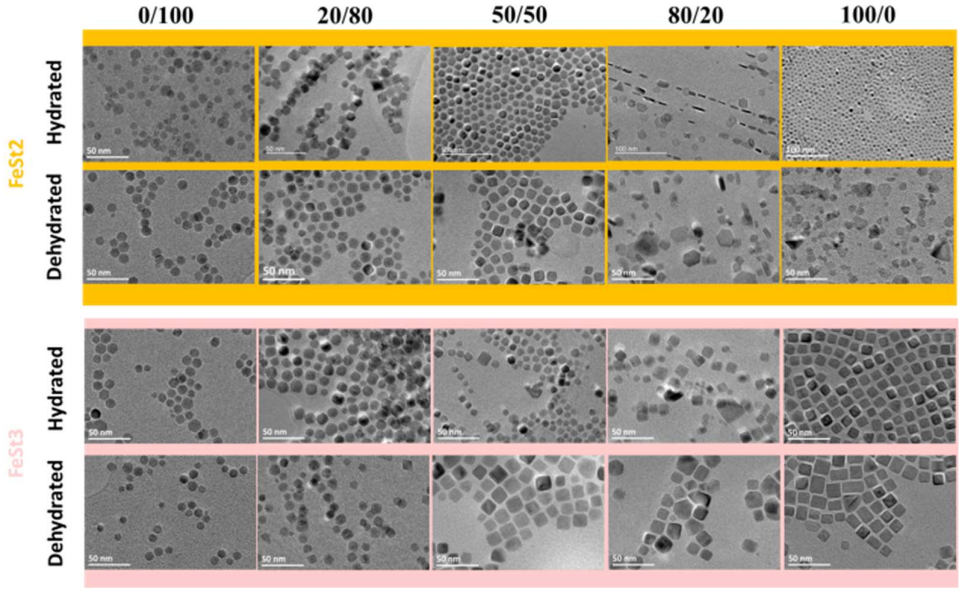

Figure 1. Influence of the ratio NaOl/OA on the shape of the NPs depending on the precursor structure and hydration degree

Figure 1 and Table 2, demonstrate clearly that the introduction of NaOl in the reactant media has an effect on the shape of NPs. The shape of the synthesized NPs being purely isotropic (spherical) only when sole OA is used as ligand. NaOl, even if added in low amount, triggers effectively the shape of NPs towards faceted shapes. However, the evolution of the shape with the amount of NaOl is not the same for all iron stearates and depends strongly on the nature of stearates, $FeSt_2$ and $FeSt_3$, and on their hydration degree.

Interestingly, specific shapes are preferentially obtained from a given precursor structure. At low ratio, less rounded NPs are obtained for all precursors. When the ratio increases, $FeSt_2$ and $FeSt_{2,d}$ allowed to easily obtain nanoplates when it was not possible with $FeSt_3$ and $FeSt_{3,d}$ that led preferentially and quite easily to nanocubes.

At the NaOl/OA ratio of 50/50, faceted NPs or deformed nanocubes are obtained with $FeSt_3$ and $FeSt_2$. At the NaOl/OA ratio of 80/20, $FeSt_3$ which is more hydrated than $FeSt_2$ led to faceted NPs when plates are obtained with $FeSt_2$ (Table 1). At 100/0, ultra-small faceted NPs are obtained with $FeSt_2$ when nanocubes are synthesized with $FeSt_3$.

By contrast with our previous study investigating only the 50/50 ratio and showing that only dehydrated stearates led to the cubic shape[35], nanocubes were obtained here with hydrated $FeSt_3$ just by increasing the amount of NaOl. That confirms that one parameter which hampers the formation of nanocube is the availability of the oleate ligands. However, $FeSt_2$ which is less hydrated than FeSt3 did not lead to nanocubes but rather to nanoplates.

With dehydrated iron stearates $FeSt_{2,d}$ and $FeSt_{3,d}$, well defined faceted NPs are obtained with lower amounts of introduced NaOl. By the NaOl/OA ratio of 50/50, nanocubes are obtained with both dehydrated stearates. For the higher NaOl/OA ratio, shaper edged cubes were obtained for $FeSt_3$ when plates are obtained with $FeSt_2$.

The difficulty in obtaining NPs with defined and homogeneous shapes with hydrated iron stearate (need of a higher amount of NaOl) confirmed that NaOl interacted with water and thus it cannot absorb on specific faces of nucleus to trigger the growth of given shape. It is well-known that NaOl formed easily water micelles at low concentration as it has a low critical micellar concentration (CMC) in water[46]. Therefore, when the amount of NaOl increases, faceted NPs are at first form and then more defined shapes appear at ratio which depend on the water content. That would explain why nanocubes are obtained for a NaOl/OA ratio of 100/0 with the hydrated $FeSt_3$ but at a NaOl/OA ratio of 50/50 for the dehydrated one. That confirms that the water content is a parameter that required to be carefully monitored for the synthesis of homogenous and shape defined NPs.

However, $FeSt_3$ whatever its hydration rate leads to nanocubes by adjusting the NaOl amount when $FeSt_2$ whatever its hydration rate, conducts to nanoplates when the amount of NaOl increases (even if some cubic shape NPs are observed to form for a ratio 50/50). Therefore, the structure of the precursor has an influence on the final shape.

The main difference between $FeSt_2$ and $FeSt_3$ are their water content and also the amount of stearate chains which is higher with $FeSt_3$ than $FeSt_2$. From our previous study, the kinetic of decomposition of $FeSt_2$ is faster than that of $FeSt_3$ which occurs on a larger range of temperature. From experiments with only oleic acid or NaOl in the reaction mixture, the mean size of NPs seems to be lower for $FeSt_2$ with NaOl by comparison with OA which suggests that NaOl would favor the decomposition of $FeSt_2$ at lower temperature providing larger amount of monomer. It is a first result as, by contrast, oleic acid is well-known to stabilize the iron precursor[18,47]. That suggests that the cubic growth

is favored by a slow generation of monomer when the 2D growth would prefer a quicker generation of monomer. It has already been reported that the cubic growth is favored by a low heating rate[47,48]. However how can we explain why nanocubes are preferentially formed with $FeSt_3$ stearates when nanoplates are obtained with $FeSt_2$ precursors ?

At first, we may consider the theory of the shape control through ligand absorption which is quite simple. The crystallographic planes of fcc materials such as magnetite don't present the same surface energy γ. Typically, the ranking established from the lowest energy planes is $\gamma_{\{111\}} < \gamma_{\{100\}} < \gamma_{\{110\}} < \gamma_{\{hkl\}}$ (with h,k,l>1)[22,23]. When a nucleus is formed, it should be then enclosed by the {111} planes that present the lowest surface energy. Thus, a cube which is enclosed by {100} planes wouldn't be favored. But as for a given volume, the surface of a cube is lower than the one of an octahedron. The stable nucleus is thus a compromise with the presence of both planes families to reduce the surface energy: the cuboctahedron. Depending on the synthesis conditions, twin defects can also occur in the nucleus. The presence of defect in the nucleus will have a major effect on the final shape of the nanocrystal. For example, a mirror (111) plane can lead to flat nanoparticles[24]. The nucleus shape and structure appear thus major for the further shape control[49,50].

The role of the ligands in the shape control has been ascribed to the tuning of growth rate of certain planes[4,17]. E.g. the adsorption of a ligand on {111} planes of a cuboctahedron nucleus will reduce their growth rate. The {100} planes will grow faster leading to their disappearance. The final shape will then be an octahedron. Rath and al[25] showed through simulation that the {111} plane family of magnetite has a most active surface for adsorption than the {311} and {110}. When a chelating ligand such as oleate is present, it would then adsorbate on the {111} planes of the nuclei reducing its growth rate.

As it has been widely reported that the adsportion of oleate on specific faces of nuclei is responsible for the cubic shape, one hypothesis would be that $FeSt_3$ precursors provide more deprotonated carboxylic acid based ligands (oleate from NaOl and stearate from $FeSt_3$) which are necessary to drive the cubic growth of nuclei. However nanocubes were synthesized with dehydrated $FeSt_2$ and a ratio of 50 and nanoplates were formed with higher ratios. In addition $FeSt_3$ and $FeSt_{3,d}$ are "more hydrated than $FeSt_2$ and thus deprotonated ligands are not all available. One may suppose that with FeSt2 and FeSt2,d, the available ligands favour the nanoplates formation.

The synthesis mechanism of iron oxide nanoplates is not clearly elucidated and their synthesis is still a challenge. Most reported nanoplates have been synthesized by hydrothermal process but some nanoplates have been synthesized by thermal decomposition of iron oleate (FeOl) in presence of NaOl in octadecene [12,53,52]. By tuning the molar ratio of NaOl/FeOl in octadecene solvent, Zhou et al[12] obtained Fe_3O_4{111} facet exposed nanoplates, truncated octahedrons, and tetrahedrons, and reported the predominant role of NaOL in preserving Fe3O4{111} facets[12]. the adsorption of Ol^- on the Fe_3O_4{111} facet is more favorable than that on the Fe_3O_4{100} facet. As a result, the growth on other facets is faster than that on the Fe_3O_4{111} facet, which results in the preservation of Fe_3O_4{111} facets in the products.

Nanocubes were obtained in solvent with higher boiling point and it was explained by the impact of NaOl on the nucleation and expitaxial growth process. NaOL may play different roles in different reaction temperatures: (i) preferentially binding onto Fe_3O_4{111} facets in low temperature octadecene solvent; (ii) delaying the nucleation effect and resulting in an expitaxial growth process in higher temperature solvent. Palchoudhury et al [52] reported that the formation of different-shaped NPs (including nanoplates) in a similar system was achieved by controlling the nucleus concentration and growth rate and the nanoplates formation was attributed to the presence of a residual product from the precursor reaction under diffusional growth conditions,.

We know that the decomposition kinetics of FeSt2 is faster than that of FeSt3 which occurs on a larger range of temperature. The nanocubes formation is established to be due to the absorption of Ol^- on specific faces but the effect of heating rate is not clear but should depend on it effects on the nucleation and growth rate (Tableau 1). Considering the above reported results for the formation of nanoplates, the nucleation and growth rates are important and we have shown that they are different between $FeSt_2$ and $FeSt_3$ which constitutes a first explanation of the nanoplate formation with $FeSt_2$.

Another parameters which seems important is the nature and amount of ligands: considering the presence of oleic acid and deprotonated carboxylic acid (oleate and stearate) and a mechanism of "fast growth assisted by precised ratio of binary surfactants" reported for the formation of gold nanoplates[51] and the presence of a residual product for nanoplate formation[52], one may suppose that the ratio of these binary surfactants (oleic acid and deprotonated carboxylic acid) is important and should be optimal to favour a plate growth. Oleic acid adsorbes less strongly (OA is a universal stabilizer on each facet[12]) than deprotonated carboxylic acid on specific faces of nuclei and their different adsorption on specific faces should also drive the plate growth. The nucleation and growth kinetics are also important and considering the formation of nanoplates only with $FeSt_2$, both kinetics have to be high.

The nanocubes and nanoplates are very interesting for biomedical applications due to their shape anisotropy. Yet, the shapes obtained in this part could be optimized in order to get a properly defined shaped before investigating their structural properties.

An optimization of the cubic shape NPs leading to octopod shape NPs

The optimization of the cubic shape of the NPs was realized in two times. At first, the influence of the heating rate on the cubic morphology was investigated. Indeed, the kinetic conditions would favor the cubic shape[28]. Several reports[12,27,28,30] showed that high heating rates were rather used for nanocube synthesis. The heating rate has been varied by using hydrated $FeSt_2$ (cheapest and easiest precursor to synthesize) at a NaOl/OA ratio of 50/50. Figure S1 present the TEM images of both syntheses which have led with a heating rate of 1°C/min to faceted

Preprints (www.preprints.org) | NOT PEER-REVIEWED | Posted: 1 October 2018 doi:10.20944/preprints201810.0006.v1

Peer-reviewed version available at *Nanomaterials* **2018**, *8*, 881; doi:10.3390/nano8110881

NPs with no specific shapes and rounded corner cubes at 5°C/min and to a decrease in the NPs mean size from 13.5 ± 2.5 nm to 11.8 ± 1.8 nm confirming that a high heating rate is favorable to the cubic shape in our synthesis conditions.

Secondly, the synthesis of nanocubes with $FeSt_3$ has conducted to rounded corner shapes by comparison with the oleate precursor leading to nanocubes with straight faces. The hypothesis being that the shape with round corners originated from a lack of the surfactant (NaOl) involved in the cubic growth control (in agreement with the presence of water molecules in the precusor). The objective was here to introduce more NaOl (i.e. increasing the ratio NaOl/$FeSt_3$) to provide more ligands to control the growth of flat faces. Therefore, the ratio Precursor/Ligands was increased from 0.75 to 1 just by adjusting the amount of $FeSt_3$. Furthermore, a high heating ramp of 15 °C/min was chosen to ensure the growth step to happen in the kinetic regime, i.e. fast enough to favor the cubic morphology which is not favored in the thermodynamic controlled conditions. TEM image in Figure 2 shows that modification of the synthesis protocol allowed improving the definition of the nanocube shape and nanocubes with a mean size of 14.5 ± 1.6 nm (NC15) were obtained.

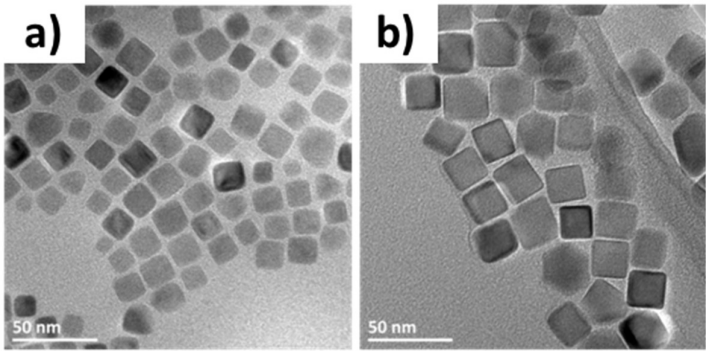

Figure 2. TEM images of cubes synthesized from $FeSt_3$ with the Kovalenko protocol a) and with the optimized protocol b)

The XRD pattern of NC15 (Figure S2.a) indicated that nanocubes are made of a core of wüstite $Fe_{1-x}O$ with a shell of spinel, as already observed[36,37]. Considering the previous observations with nanospheres, such composition may be related to the competition between the growth rate and the oxidation kinetic of the FeO nuclei within this temperature range. Lattice parameters calculated for NC15 from Rietveld refinement gave a parameter of 8.392 ± 1 Å for the shell close to that of stoichiometric magnetite (0.8396 nm, JCPDS file 19-629) and of 4.237 ± 1 Å for the wüstite core. From an earlier study on nanocubes synthesized using iron oleate as precursor[36] and from recent results to obtain nanocubes with a homogeneous spinel composition[45], the first formed phase under the used experimental conditions is the FeO one which is then oxidized with time. The shell displayed generally a lattice parameter close or slightly larger to that of stoichiometric magnetite which is ascribed to an epitaxial matching between both phases and the lattice parameter of the wüstite phase strongly depended on its oxidation state. According to the formula $Fe_{1-x}O$, the iron content x can be easily calculated from the cell parameter using the relationship $a_{FexO} = 0.3856 + 0.0478x$[54]. The result gives x value of 0.8 which suggested that the wüstite core has been formed in strong reducing conditions and even that the current synthesis conditions are stronger than that observed in our previous study (max 0.83)[36]. The wüstite phase was shown to be metastable and to transform into wüstite with higher iron content and spinel phases through an oxidation mechanism with ageing time in former nanocubes[36]. The oxidation mechanism and the epitaxial growth resulted in the diffusion of cations and vacancies that generated high strains at the AFM/FIM interface and in the FIM shell. IR spectra (Figure S2) showed that the Fe-O bands are characteristic of a slightly oxidized magnetite (presence of Fe(+II) and Fe(+III) cations). The broad band maximum is between those of the stoichiometric magnetite and maghemite phases[20].

To explain the effect of the heating rate, the core-shell $Fe_{1-x}O@Fe_{3-x}O_4$ structure of the cubes could be indicative of something quite important. Indeed, the formed nucleus is composed of $Fe_{1-x}O$ [45]. During the growth step, there is a competition between the growth of $Fe_{1-x}O$ and its oxidation as the synthesis proceeds in air and that some water molecules are present. The cubic $Fe_{1-x}O$ structure should rather favor a cubic growth and therefore an oxidation may affect this cubic growth. Thus, if the growth kinetic is larger than the oxidation kinetic, a $Fe_{1-x}O$ cubic NP is grown which oxidized afterwards. On the opposite, if the growth kinetic is smaller than the oxidation kinetics, the NPs will be fully oxidized at the end. That could explain why high heating rate are necessary to form defined nanocubes.

Different synthesis conditions have been tested in order to obtain nanocubes with a homogeneous composition in the spinel phase (i.e. without a wüstite core): bubbling of air, other solvents than alkene; among others. Unfortunately, a loss of the cubic shape was generally observed. Indeed, the synthesis conditions of the cubic shaped NPs are constrained and reducing and these strict conditions affect the oxidation kinetic. It has been often observed[31,36] that such a combination of NaOl and OA leads to core-shell cubes which suggested a strong influence of the amount of oleate chains. The environment generated by the carboxylate and/or alkenes at high temperature is certainly reducing. The nucleates have a composition close to $Fe_{1-x}O$ and the growth rate of nucleates is superior to the oxidation rate. The nice cubic shape could be attributed to this growth under the $Fe_{1-x}O$ structure. Our hypothesis is that sharply defined nanocubes are obtained in our

Preprints (www.preprints.org) | NOT PEER-REVIEWED | Posted: 1 October 2018 doi:10.20944/preprints201810.0006.v1

Peer-reviewed version available at *Nanomaterials* **2018**, *8*, 881; doi:10.3390/nano8110881

used experimental conditions only if the nucleation and growth steps occurred on NPs with a $Fe_{1-x}O$ composition. Then, $Fe_{1-x}O$ is oxidized when exposed to air leading to core-shell NPs with a magnetite shell. That would be in agreement with our previous observations during the synthesis of nanocubes using the iron oleate precursor[36].

Nevertheless, other published methods have reported nanocubes with a spinel composition.[8,9,28,33] The method developed by Pellegrino and al[8] using a mixture of squalene and dibenzylether (DBE) as a solvent has led to interesting results. They reported that the products of decomposition of the DBE were responsible for the control of the shape of the material to a full spinel phase[9]. The adapted Pellegrino protocol using iron (III) stearate and DBE as solvent led to a cubic shape with elongated corners named octopods (Figure 3) which are considered as interesting to investigate. Moreover, the fact that the octopods were oxidized indicates that the reaction media should favour the oxygen diffusion.

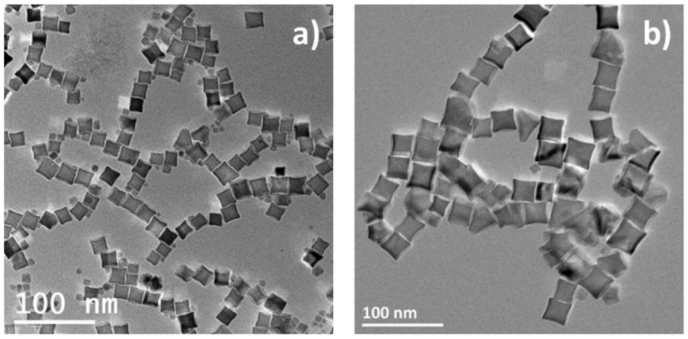

Figure 3. TEM images of the 18 nm octopods a) and 28 nm octopods b)

Such an octopod shape would originate from a difference in the kinetics of the reaction. It has been explained that when the cubic NP is formed, if the number of monomers that precipitated on the surface is large, it will preferentially remain on the corner that presented the higher surface energy instead of diffusing on the whole surface of the NPs. As the heating rate up to the growth step is rather fast (10°C/min), this could be what is at work here. In Pellegrino's protocol, the ratio DBE:squalene was demonstrated to drive size control. The more DBE was introduced, the smaller the NPs.

In our system, the size has been tuned by adapting the ratio FeSt:OA and mean sizes of 17.2 ± 2.2 nm (NO18) for a ratio of 1:3 and of 27.8 ± 4.2 nm (NO28) for a ratio of 1:4.5 were thus synthesized. These objects are quite interesting as the presence of the elongated corner should increase the shape anisotropy of NPs. They presented a homogeneous spinel composition. The XRD refinement (Figure S2.c) gave a lattice parameter of 8.364 Å for NO18 and 8.370 Å for NO28. Those lattice parameters values in-between those of magnetite and maghemite (0.8346 nm, JCPDS file 39-1346) indicated an oxidation of both NO. The indexation of the broad Fe-O band (Figure S2.d) at 580 cm^{-1} (magnetite) along with the band at 630 cm^{-1} (maghemite) is in agreement with an oxidized magnetite composition.

Due to the anisotropic shape, the crystallite size has been determined from Rietveld refinement as a function of the (hkl) planes (Table 3). The crystallites size depended on the size with the largest directions being (400) and (511) for NO28 and (220) and (440) for NO18. The longest directions for NO18 are thus the one belonging to the (110) family implying that the diagonal of the face is longer than the diagonal of the assimilated cube. For NO28, the longest direction is the (400) one followed by the (511) one which indicates a different exposition of crystallographic planes in the corner

Table 3. TEM size and lattice parameter and crystallites size determined from XRD refinement

Sample	TEM (nm)	Lattice parameter (Å)	Crystallite size (nm)										
			220	311	222	400	331	422	511	333	440	531	442
NO18	17.2 ± 2.2	8.364	15	13	11	11	11	12	13	11	15	12	11
NO28	27.8 ± 4.2	8.370	19	20	13	25	18	17	23	12	19	21	16
NPl17	16.7 ± 5.2	8.384	11	9	17	8	11	10	8	17	11	9	12

Exploring the nanoplates synthesis

Previously, all conditions lead to the same plate thickness (around 6 nm). To tune this thickness in order to modulate the properties of the objects, the heating rate has been varied. With a NaOl/OA ratio of 80/20 and whatever the heating rate (Figure S3), nanoplates are obtained. The mean sizes are for 1°C/min: l=16.7± 5.2 nm and t=8.6 ±1.7 nm and for 5°C/min: l=16.6 ± 4.9 nm and t=6.1 ± 1 nm): the thickness decreased with the increase in the heating rate. An increase in the heating rate up to 10 °C/min promoted partly the formation of cubic NPs (Figure 7). At 10 °C/min, the length decreased (15.8 ± 4.5 nm) and the thickness is in between the two former values (7.1 ± 1.4 nm). Yet, the variation is not significant in regard of the measurement error. Thus, there is no variation of the thickness with the heating rate.

As the nanoplates shape didn't' present the same dependence on the heating rate than the cubic one, one may suppose that the main step to control the nanoplates shape is not the growth step (case of nanocubes) but rather the nucleation one. We have thus introduced a "nucleation step" in our experimental conditions of nanoplates synthesis and we have varied the "nucleation step" temperature. When this step was removed or was below 200 °C, nanoplates were observed to form (Figure 4). Above 200°C, the nanoplate's occurrence decreased. Moreover, when the duration of the step was increased from 10 to 30 min at 210°C, no plates were observed at all (Figure 4). That confirms the importance of the nucleation step.

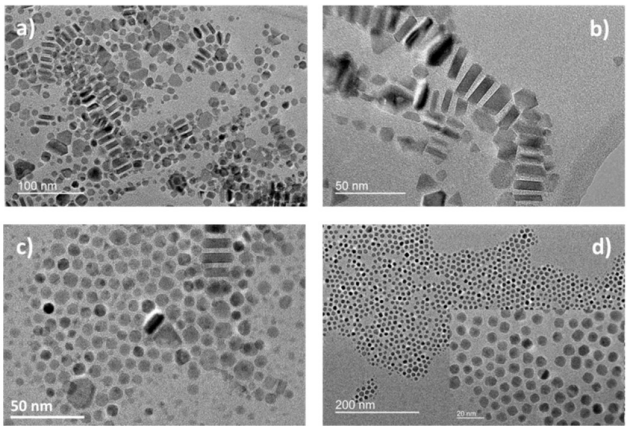

Figure 4. Influence of the germination step with the ratio 80/20: no germination step a), germination step at b) 190 °C for 10 min, c) 210 °C for 10 min and d) 210°C for 30 min

High resolution TEM (HR-TEM) and 3D TEM tomography have already been performed earlier on nanocubes to confirm their shape[36]. They were performed here on the nanoplates as this shape has been rarely reported.

Preprints (www.preprints.org) | NOT PEER-REVIEWED | Posted: 1 October 2018 doi:10.20944/preprints201810.0006.v1

Peer-reviewed version available at *Nanomaterials* **2018**, *8*, 881; doi:10.3390/nano8110881

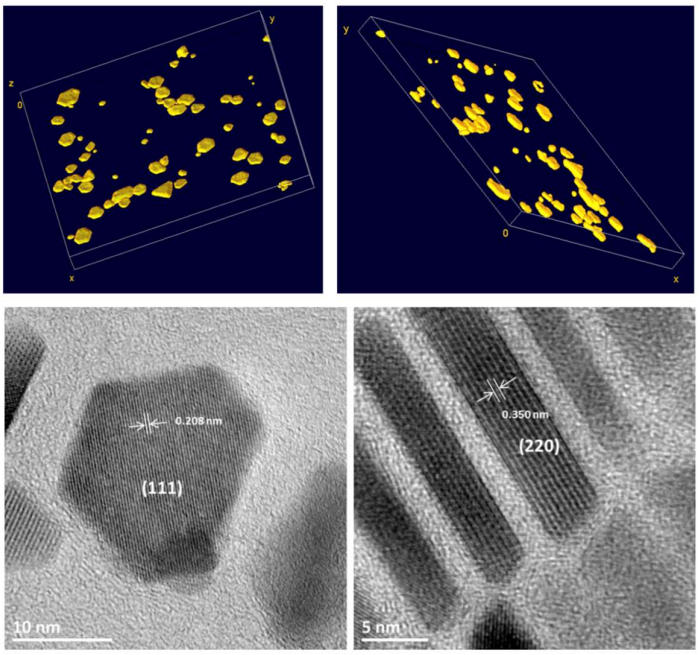

Figure 5. 3D TEM reconstruction of the nanoplates (top panel) and HR-TEM images of the long face of a platelets (left) and of the side (right) (bottom panel).

The 3D TEM tomography images in Figure 5 confirmed the flat shape of nanoplates and showed that the fully formed nanoplates are not perfectly flat but concave. The smaller NPs are rather convex confirming the spherical profile to reduce the surface energy. The plates studied here have a 17.5 ± 4.4 nm length and a 6.3 ±1.3 nm thickness (nanoplates from hydrated $FeSt_2$). HR-TEM (Figure 5) showed that the long face of the plate is made out of {111} planes when the sides are made out of {220} planes.

The XRD pattern (Figure S2.c) presented the peaks characteristic of a spinel phase with a lattice parameter of 8.384 ± 1 Å, determined through Rietveld refinement. The nanoplates are thus slightly oxidized in agreement with the IR spectrum (Figure S2.e) where a broad band with a maximum at 580 cm^{-1} (close to the magnetite one) is observed. The crystallite size according to specific crystallographic directions was also determined by Rietveld refinement (Table 3). The crystallite size of 17 nm in the direction <111> is in agreement with a 2D growth formation mechanism and TEM study. As most of the plates tended to lay flat during the XRD acquisition. It is hard to clearly see the planes within the thickness. Yet the value of 8 nm close to the one measured for the thickness would imply that the planes (400), (511) enclose the sides of the plates.

We have shown above that high heating rates were required to favor the cubic shape when it was not the case for the nanoplate formation. Contrarily to the cubes they don't present a reduced phase core of wüstite. However, plates whose thickness is very small should be easily oxidized when exposed to air despite the growth kinetics. In fact, the $Fe_{1-x}O$ nucleus would not be the limiting step for nanoplate synthesis.

Conclusions

The influence of the structure of the precursor on the shape of the NPs has been scarcely investigated in the literature. We have thus studied the thermal decomposition of hydrated and dehydrated $FeSt_2$ and $FeSt_3$ as a function of the amount of NaOl introduced in the reaction mixture. We have mainly confirmed that 1) NaOl triggered effectively the NPs shape formation, that 2) the nature of the precursor affects the shape with $FeSt_2$ favouring the formation of nanoplates whhen $FeSt_3$ favored that of nanocubes and that 3) the hydration is deleterious for the formation of anisotropic shapes and more NaOl is needed to form anisotropic shaped NPs from highly hydrated precursors most likely due to the interaction of ligands with water to form micelles. Thus, dehydrated precursors allowed a better control over the shape. The formation of nanocubes formation was confirmed to be driven by the amount of soduim oleate and the heating rate. The control of the monomer formation at the nucleation step was found very important for the nanoplate synthesis. Therefore, the nucleation step appeared very important to direct the nanoplate formation. The impact of an oleic acid/oleate ratio on the nanoplate shape is not to exclude.

Conflicts of interest

There are no conflicts to declar.

Acknowledgements

The Région Alsace, France, and the Labex Chimie des Sytèmes Complexes, University of Strasbourg, France are gratefully acknowledged for the doctoral fellowship to Geoffrey Cotin. This research project was also co-funded by Labex CSC, Alsace contre le cancer, INCA (project PRTK14, THERAMAG 2014-225) and the INTERREG project NANOTRANSMED. The authors thank

COST Radiomag, INCA, INTERREG , Labex CSC

Notes and references

1 F. N. Sayed and V. Polshettiwar, *Scientific Reports*, 2015, **5**, 9733.
2 V. Polshettiwar, B. Baruwati and R. S. Varma, *ACS Nano*, 2009, **3**, 728–736.
3 C. de Montferrand, L. Hu, I. Milosevic, V. Russier, D. Bonnin, L. Motte, A. Brioude and Y. Lalatonne, *Acta Biomaterialia*, 2013, **9**, 6150–6157.
4 E. Wetterskog, M. Agthe, A. Mayence, J. Grins, D. Wang, S. Rana, A. Ahniyaz, G. Salazar-Alvarez and L. Bergström, *Sci Technol Adv Mater*, , DOI:10.1088/1468-6996/15/5/055010.
5 C. Blanco-Andujar, A. Walter, G. Cotin, C. Bordeianu, D. Mertz, D. Felder-Flesch and S. Begin-Colin, *Nanomedicine (Lond)*, 2016, **11**, 1889–1910.
6 W. Xie, Z. Guo, F. Gao, Q. Gao, D. Wang, B. Liaw, Q. Cai, X. Sun, X. Wang and L. Zhao, *Theranostics*, 2018, **8**, 3284–3307.
7 Z. Nemati, J. Alonso, I. Rodrigo, R. Das, E. Garaio, J. Á. García, I. Orue, M.-H. Phan and H. Srikanth, *J. Phys. Chem. C*, 2018, **122**, 2367–2381.
8 P. Guardia, R. Di Corato, L. Lartigue, C. Wilhelm, A. Espinosa, M. Garcia-Hernandez, F. Gazeau, L. Manna and T. Pellegrino, *ACS Nano*, 2012, **6**, 3080–3091.
9 P. Guardia, A. Riedinger, S. Nitti, G. Pugliese, S. Marras, A. Genovese, M. Materia, C. Lefevre, L. Manna and T. Pellegrino, *J. Mater. Chem. B*, , DOI:10.1039/C4TB00061G.
10 E. Wetterskog, C.-W. Tai, J. Grins, L. Bergström and G. Salazar-Alvarez, *ACS Nano*, 2013, **7**, 7132–7144.
11 N. Lee, Y. Choi, Y. Lee, M. Park, W. K. Moon, S. H. Choi and T. Hyeon, *Nano Letters*, 2012, **12**, 3127–3131.
12 Z. Zhou, X. Zhu, D. Wu, Q. Chen, D. Huang, C. Sun, J. Xin, K. Ni and J. Gao, *Chemistry of Materials*, 2015, **27**, 3505–3515.
13 Z. Zhao, Z. Zhou, J. Bao, Z. Wang, J. Hu, X. Chi, K. Ni, R. Wang, X. Chen, Z. Chen and J. Gao, *Nat Commun*, 2013, **4**, 2266.
14 S. Sun and H. Zeng, *J. Am. Chem. Soc.*, 2002, **124**, 8204–8205.
15 T. Hyeon, S. S. Lee, J. Park, Y. Chung and H. B. Na, *Journal of the American Chemical Society*, 2001, **123**, 12798–12801.
16 J. Park, K. An, Y. Hwang, J.-G. Park, H.-J. Noh, J.-Y. Kim, J.-H. Park, N.-M. Hwang and T. Hyeon, *Nat Mater*, 2004, **3**, 891–895.
17 M. V. Kovalenko, M. I. Bodnarchuk, R. T. Lechner, G. Hesser, F. Schäffler and W. Heiss, *J. Am. Chem. Soc.*, 2007, **129**, 6352–6353.
18 L. M. Bronstein, X. Huang, J. Retrum, A. Schmucker, M. Pink, B. D. Stein and B. Dragnea, *Chem. Mater.*, 2007, **19**, 3624–3632.
19 V. K. LaMer and R. H. Dinegar, *J. Am. Chem. Soc.*, 1950, **72**, 4847–4854.
20 W. Baaziz, B. P. Pichon, S. Fleutot, Y. Liu, C. Lefevre, J.-M. Greneche, M. Toumi, T. Mhiri and S. Begin-Colin, *J.*

Phys. Chem. C, 2014, **118**, 3795–3810.
21 S. G. Kwon, Y. Piao, J. Park, S. Angappane, Y. Jo, N.-M. Hwang, J.-G. Park and T. Hyeon, *J. Am. Chem. Soc.*, 2007, **129**, 12571–12584.
22 Z. L. Wang, *J. Phys. Chem. B*, 2000, **104**, 1153–1175.
23 C. Yang, J. Wu and Y. Hou, *Chemical Communications*, 2011, **47**, 5130.
24 Y. Xia, Y. Xiong, B. Lim and S. E. Skrabalak, *Angew. Chem. Int. Ed. Engl.*, 2009, **48**, 60–103.
25 S. S. Rath, N. Sinha, H. Sahoo, B. Das and B. K. Mishra, *Applied Surface Science*, DOI:10.1016/j.apsusc.2014.01.014.
26 P. Guardia, A. Labarta and X. Batlle, *The Journal of Physical Chemistry C*, 2011, **115**, 390–396.
27 A. Shavel and L. M. Liz-Marzán, *Phys. Chem. Chem. Phys.*, 2009, **11**, 3762–3766.
28 D. Kim, N. Lee, M. Park, B. H. Kim, K. An and T. Hyeon, *Journal of the American Chemical Society*, 2009, **131**, 454–455.
29 P. Guardia, A. Riedinger, S. Nitti, G. Pugliese, S. Marras, A. Genovese, M. E. Materia, C. Lefevre, L. Manna and T. Pellegrino, *Journal of Materials Chemistry B*, 2014, **2**, 4426.
30 A. Shavel, B. Rodríguez-González, M. Spasova, M. Farle and L. M. Liz-Marzán, *Adv. Funct. Mater.*, 2007, **17**, 3870–3876.
31 H. T. Hai, H. T. Yang, H. Kura, D. Hasegawa, Y. Ogata, M. Takahashi and T. Ogawa, *Journal of Colloid and Interface Science*, 2010, **346**, 37–42.
32 D. Kim, J. Park, K. An, N.-K. Yang, J.-G. Park and T. Hyeon, *Journal of the American Chemical Society*, 2007, **129**, 5812–5813.
33 H. Yang, T. Ogawa, D. Hasegawa and M. Takahashi, *Journal of Applied Physics*, 2008, **103**, 07D526.
34 A. Cervadoro, M. Cho, J. Key, C. Cooper, C. Stigliano, S. Aryal, A. Brazdeikis, J. F. Leary and P. Decuzzi, *ACS Applied Materials & Interfaces*, 2014, **6**, 12939–12946.
35 G. Cotin, C. Kiefer, F. Perton, M. Boero, B. Özdamar, A. Bouzid, G. Ori, C. Massobrio, D. Begin, B. Pichon, D. Mertz and S. Begin-Colin, *ACS Appl. Nano Mater.*, 2018, **1**, 4306–4316.
36 B. P. Pichon, O. Gerber, C. Lefevre, I. Florea, S. Fleutot, W. Baaziz, M. Pauly, M. Ohlmann, C. Ulhaq, O. Ersen, V. Pierron-Bohnes, P. Panissod, M. Drillon and S. Begin-Colin, *Chem. Mater.*, 2011, **23**, 2886–2900.
37 A. Walter, C. Billotey, A. Garofalo, C. Ulhaq-Bouillet, C. Lefèvre, J. Taleb, S. Laurent, L. Vander Elst, R. N. Muller, L. Lartigue, F. Gazeau, D. Felder-Flesch and S. Begin-Colin, *Chem. Mater.*, 2014, **26**, 5252–5264.
38 L. M. Bronstein, J. E. Atkinson, A. G. Malyutin, F. Kidwai, B. D. Stein, D. G. Morgan, J. M. Perry and J. A. Karty, *Langmuir*, 2011, **27**, 3044–3050.
39 M. R. Buck, A. J. Biacchi and R. E. Schaak, *Chemistry of Materials*, 2014, **26**, 1492–1499.
40 Z. Xu, C. Shen, Y. Tian, X. Shi and H.-J. Gao, *Nanoscale*, 2010, **2**, 1027–1032.
41 Y. Yin and A. P. Alivisatos, *Nature*, 2005, **437**, 664–670.
42 J. Rodríguez-Carvajal, *Physica B: Condensed Matter*, 1993, **192**, 55–69.
43 A. Le Bail, H. Duroy and J. L. Fourquet, *Materials Research Bulletin*, 1988, **23**, 447–452.
44 S. Costanzo, G. Simon, J. Richardi, P. Colomban and I. Lisiecki, *J. Phys. Chem. C*, 2016, **120**, 22054–22061.
45 W. Baaziz et al, *CrystEngComm,* under revision
46 N. Mahieu, D. Canet, J. M. Cases and J. C. Boubel, *J. Phys. Chem.*, 1991, **95**, 1844–1846.
47 L. Wu, A. Mendoza-Garcia, Q. Li and S. Sun, *Chem. Rev.*, 2016, **116**, 10473–10512.
48 Q. Song and Z. J. Zhang, *Journal of the American Chemical Society*, 2004, **126**, 6164–6168.
49 T. Tan, L. Yao, H. Liu, C. Li and C. Wang, *Chemistry – A European Journal*, 2017, **23**, 10001–10006.
50 D. Gao, D. Tian, B. Chong, X. Zhang and W. Gao, *CrystEngComm*, 2014, **16**, 7106–7114.
51 C. Wang, C. Kan, J. Zhu, X. Zeng, X. Wang, H. Li and D. Shi, *Journal of Nanomaterials*, 2010, **2010**, 1–9.

52 S. Palchoudhury, Y. Xu, A. Rushdi, R. A. Holler and Y. Bao, *Chemical Communications*, 2012, **48**, 10499.

53 Z. Zhou, Z. Zhao, H. Zhang, Z. Wang, X. Chen, R. Wang, Z. Chen and J. Gao, *ACS Nano*, 2014, **8**, 7976–7985.

54 C. A. McCammon and L. Liu, *Phys Chem Minerals*, 1984, **10**, 106–113.

55 M. Park, N. Lee, S. H. Choi, K. An, S.-H. Yu, J. H. Kim, S.-H. Kwon, D. Kim, H. Kim, S.-I. Baek, T.-Y. Ahn, O. K. Park, J. S. Son, Y.-E. Sung, Y.-W. Kim, Z. Wang, N. Pinna and T. Hyeon, *Chemistry of Materials*, 2011, **23**, 3318–3324.

Preprints (www.preprints.org) | NOT PEER-REVIEWED | Posted: 1 October 2018 doi:10.20944/preprints201810.0006.v1

Peer-reviewed version available at *Nanomaterials* **2018**, *8*, 881; doi:10.3390/nano8110881

ESI

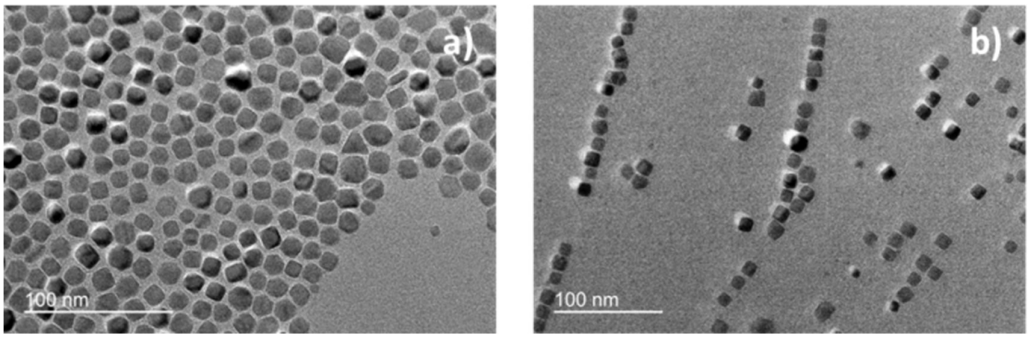

Figure S1. TEM images of the decomposition of hydrated $FeSt_2$ at a NaOl/OA ratio of 50/50 with a heating rate of a) 1°C/min and b) 5°C/min

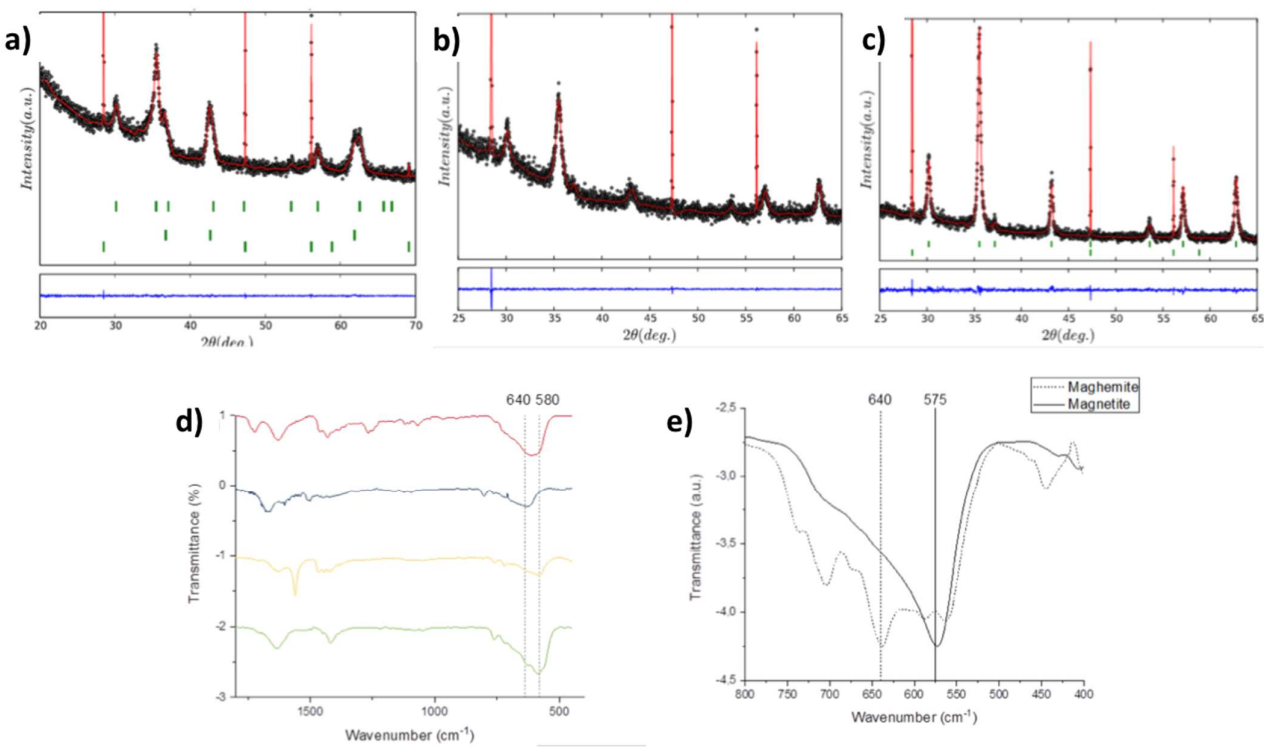

Figure S2. XRD refinement of NC15 a), NPl b), NO28 c)-, IR spectra of NC (blue), NPl (yellow) and NO28 (green) d) and typical IR spectra of slightly oxidized magnetite and maghemite e).

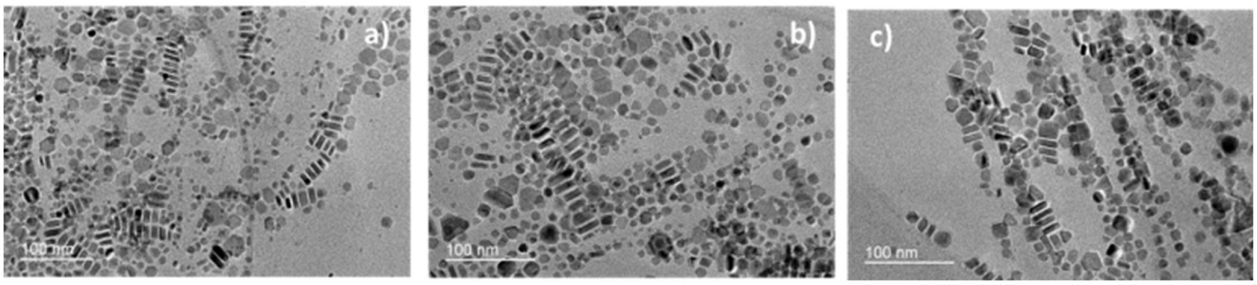

Figure S3. TEM images of the decomposition of hydrated $FeSt_2$ at a NaOl/OA Ratio 80/20 a) 1°C/min, b) 5°C/min and c) 10 °C/min